

Visualization of Secondary Flow in a Corner of a Channel

Jindřich Bém¹⁾, Daniel Duda^{1, a)}, Jiří Kovařík¹⁾, Vitalii Yanovych¹⁾ and Václav Uruba^{1, 2, b)}

¹⁾Faculty of Mechanical Engineering,
University of West Bohemia in Pilsen,
Univerzitní 22, 306 14 Pilsen, Czech Republic

²⁾Institute of Thermodynamics,
Czech Academy of Sciences,
Dolejškova 5, 182 00, Prague, Czech Republic.

^{a)}Corresponding author: dudad@kke.zcu.cz

^{b)}uruba@kke.zcu.cz

Abstract. We report observation of secondary flow in one corner of developing channel air flow. Length of the channel, i.e. length of boundary layer, is 400 mm, which is 3.2 times the channel cross-sectional size. Three components of velocity are measured by using a Stereo Particle Image Velocimetry (PIV) technique in the measurement area of size 24×22 mm, which is perpendicular to the direction of main flow in the channel. The Reynolds number based on the length of the channel ranged from $4 \cdot 10^4$ to $8 \cdot 10^5$ and has been controlled via imposed velocity. At low Reynolds number we observe a laminar corner vortex having at all velocities the same orientation. This symmetry breaking is probably caused by an imperfectness of the experimental device. At Reynolds number around $8 \cdot 10^4$ this vortex starts to slightly vary its strength and position causing transition of boundary layers into turbulence at $Re = 1.1 \cdot 10^5$. At higher Re this laminar vortex disappears from the instantaneous velocity fields, but it is still apparent in the averaged ones. It gets smaller and another oppositely oriented vortex forms; note that the second vortex is not observed in the instantaneous velocity fields, only in the ensemble average. At even higher Re , this secondary flow structure is smaller than the turbulent boundary layers, but its shape of a pair of counter-rotating vortices is conserved probably being a seed for secondary flow between fully developed boundary layers reported in the literature for longer channels with fully developed flow.

INTRODUCTION

The turbines gain angular momentum from the energy of working medium (steam, water, air...) by using two complementary mechanisms: first the *impulse* mechanism based on bending the flow direction in an interblade channel, second the *reaction* mechanism based on accelerating the fluid in the interblade channel. Thus the understanding of flow inside such a channel is very important in order to limit the energy losses caused by many different physical or technical effects. Among the physical ones let's focus on the various *secondary flows*, which are stable flow structures superimposed on the ideal flow geometry [1].

First, the bending of the channel leads to *centrifugal* instability which give rise to so-called *Görtler vortices* [2]; this mechanism applies in more famous *Taylor-Couette instability* in case of flow between rotating cylinders [3].

Second, the effects of *boundary layer interactions* lead to *secondary flows of second kind*. One example of this class of flows is the *passage vortex*, which born, when the end-wall boundary layer meets with the leading edge [4]. When two perpendicular boundary layers (at end-wall and at blade) interact, there can arise a corner vortex, or a system of vortices, in dependence on the Reynolds number [5]. The nature of this secondary flow of second kind is mainly studied in case of *long* channel or duct [6], where the flow is already *developed* (i.e. the boundary layers met filling the entire cross-section of the channel), while in the case of turbine blade, the channel is *short*.

Therefore, in our study we focus to the corner of *short* channel (length is 3.2 times the width), which is *straight* in order to not mismatch the first- and second-kind secondary flows.

Reynolds Number

In this problem we define *Reynolds number* as

$$Re_L = \frac{WL}{\nu} \quad (1)$$

where W is the imposed velocity, L is length of the channel and ν is the kinematic viscosity of air. This definition follows the standards in boundary layer studies rather than those in secondary flow studies, because the later are usually performed in the case of long channel with fully developed flow. Hence, the natural choice of relevant length-scale of the problem is the width (or *hydraulic diameter*) of the channel. In our case, the channel flow is not fully developed, therefore the natural choice of relevant length-scale would be the boundary layer thickness, which limits the size of vortices. In order to consistency with the boundary layer studies we have chosen their definition of Reynolds number based on the distance from boundary layer origin, which is the length of the channel.

EXPERIMENTAL SETUP

Wind tunnel is consisting from three main parts. First part is radial compressor that suck air from outside space and push it through next part. Second part is chamber with gratings. It secures create small vortexes and in outcome it is creating laminar flow that enter in next part. Third part is empty quad shaped measurement section with length 400 mm and cross-sectional size 125×125 mm. This part has been created by using Plexiglas. Air flowing in wind tunnel is escaping thru outlet in to atmosphere. Outlet is located at the end of measuring section.

Stereo Particle Image Velocimetry (PIV) is technique for measuring all three velocity components of flowing fluid in one plain. For visualization of air flow is using generator that create smoke. The smoke contains tiny particles made from SAFEX. For best results is necessary that density of smoke is in optimal level. In fact, by this method has been measured velocity of particles instead velocity of flowing fluid. Inertia mass is scaled by the third power of size and Stokes' drag is scaled by the first power of size therefore viscosity dominates relative motion of particle. Therefore it allows measure speed of flowing fluid via particles observation.

Laser contain separated two lasers and it allows to create delayed two short pulses. Minimum delay time is $(1.5 \mu s)$. Measuring plain is created by using lasers beams that are spreaded by cylindrical lens into one thin light plain. Laser pulses are reflected on tiny particles. Measuring plain is perpendicular to direction of main flow speed.

Cameras are mounted in front of measurement section with view "upstream" fluid flow. Cameras are working in double frame mode. It means they take two delayed images with same delay like laser blinking.

Images taken by cameras are process in Dynamic studio with Dantec adaptive PIV. Velocity of flowing fluid is calculated in small subsections by using cross correlation function.

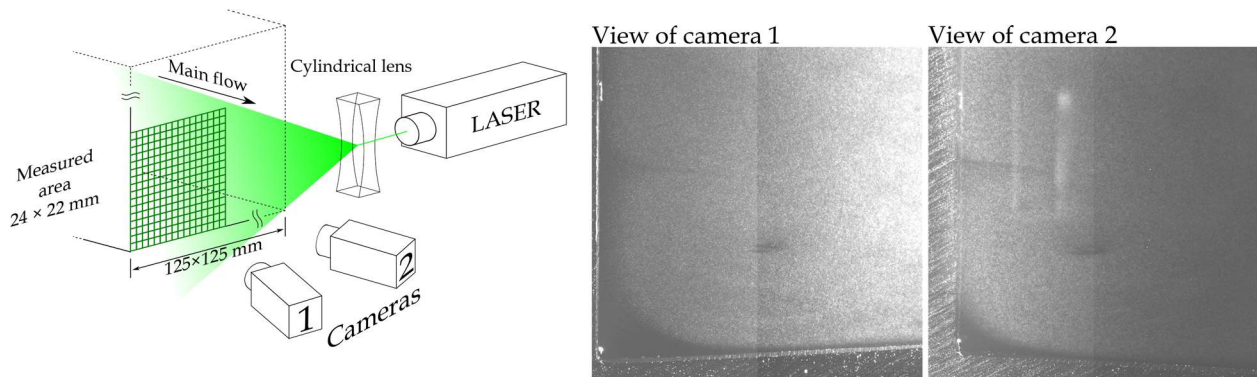


FIGURE 1. Experimental setup. The air velocity is measured in a plane perpendicular to the main flow at the open end of the wind tunnel test section of length 400 mm. Two cameras are used in the Scheimpflug setup each observing the same scene from different angles. Example of the rough images taken by the cameras is in the right-hand-side of this figure.

RESULTS

Laminar Secondary Flow

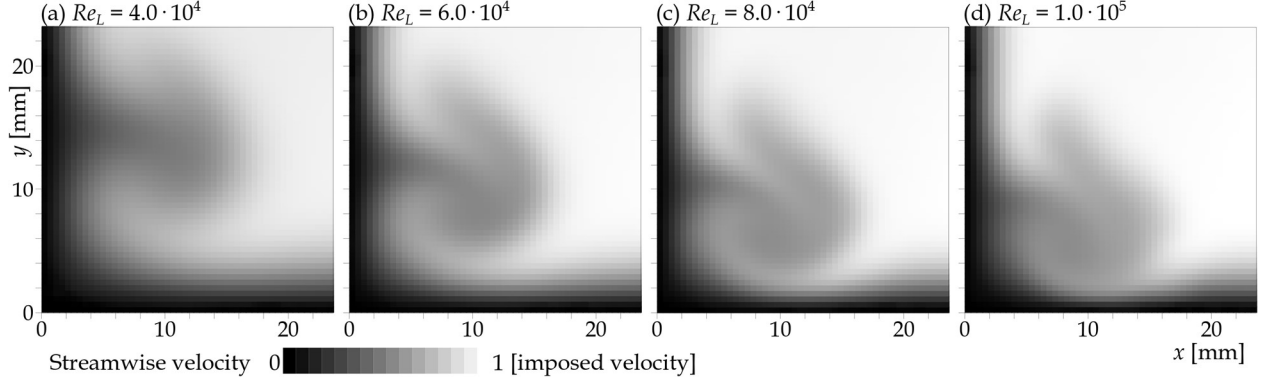


FIGURE 2. Ensemble-averaged measured spatial distribution of the streamwise velocity (perpendicular to the studied area) at four different Reynolds numbers in the *laminar regime* of secondary flow. The channel corner is in the bottom left corner of the figures; black color represents the zero streamwise velocity, while the white one plays for streamwise velocity equal to the imposed velocity. Note that the corner vortex is laminar and it ejects the low-momentum material into the main flow.

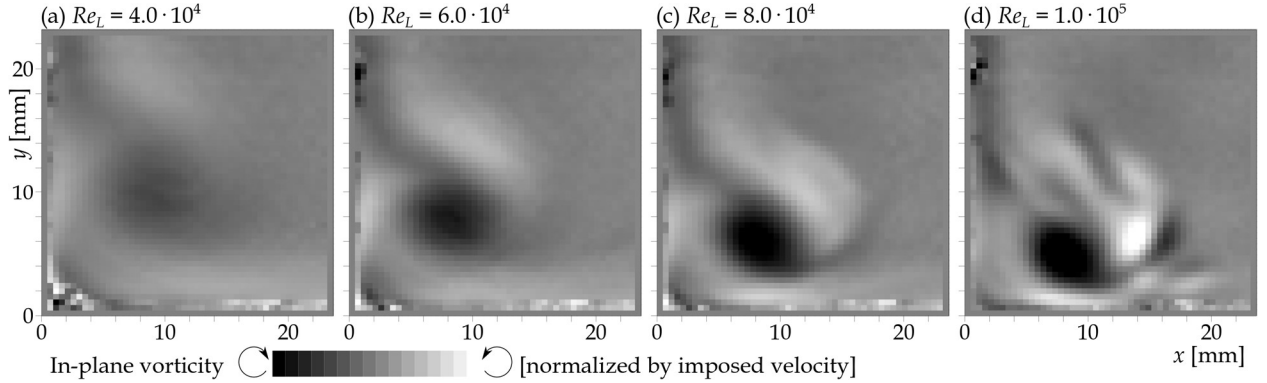


FIGURE 3. Ensemble-averaged spatial distribution of the in-plane vorticity at four different Reynolds numbers same as in the Fig 2. We apologize for higher noise close to the corner and at the wall. The vortex orientation was equal in all measured cases, where this single laminar vortex existed, although according to [5], the orientation should randomly switch in the fully symmetric case. This symmetry breaking can be caused by arbitrarily small deviation, which very probably occur in our physical experimental stand.

Figures 2 and 3 shows a single laminar vortex in the corner of the channel (which is in bottom left corner of the figures). We can observe that with increasing velocity, the vortex approaches the wall, gets smaller but stronger (faster than the linear scaling with velocity), all these trends are displayed also in Figure 4 as a function of Reynolds number based on the channel length. The vortex parameters are obtained via fitting the velocity field with the Gaussian vortex with tangential velocity profile

$$u_{\vartheta}(r) = \frac{\Gamma}{2\pi R^2} \cdot r \cdot e^{-\frac{1}{2}\left(\frac{r}{R}\right)^2} \quad (2)$$

where r is the distance from vortex center, R is the vortex core radius and Γ is its circulation. The radius R and circulation Γ together with the location of vortex center x_c and y_c are the fitting parameters of the algorithm described in our previous work [7].

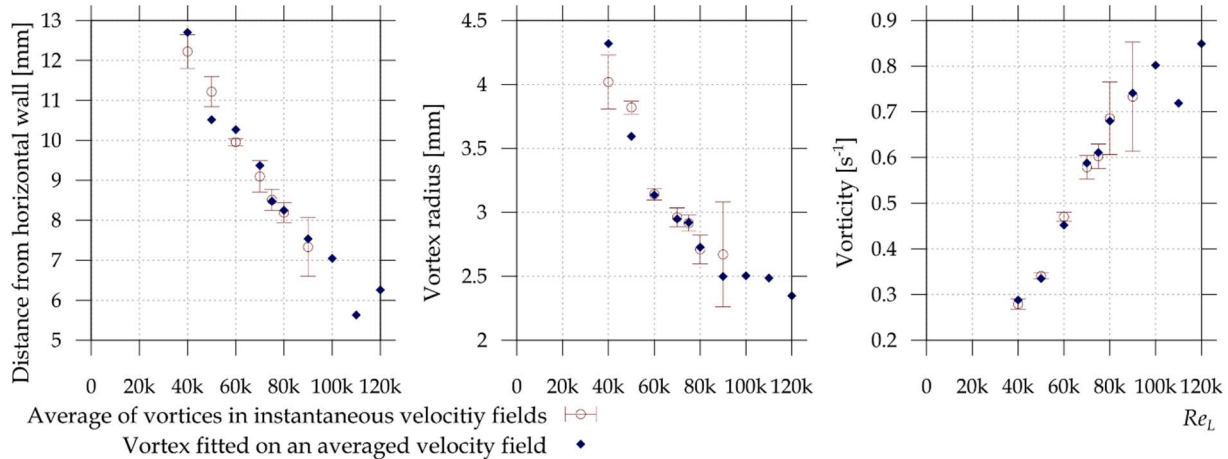


FIGURE 4. Properties of large laminar vortex for Re_L smaller than $1,2 \cdot 10^5$. Red circles represent the average of laminar vortex fitted on instantaneous velocity fields, the largest Re_L , for which this approach has been possible is $9,0 \cdot 10^4$, at larger Re_L there are more vortices and it is not possible to determine the “correct” one. On the other hand, fitting the vortex in averaged velocity field (that shown in Fig 2 and 3) is possible up to $Re_L = 1,2 \cdot 10^5$ and this results are shown as filled blue squares rotated by 45° .

The laminar core vortices have been fitted in both: the instantaneous velocity fields (results shown as empty red circles in Figure 4), and in the averaged velocity field (filled blue squares in Figure 4), which shows the structure, whose appearance is not needed none of the instantaneous velocity fields. Figure 5 shows an example of 4 randomly selected instantaneous velocity fields, whose shape *differ* one from each other and from the averaged structure (Figure 3d) as well. On the other hand, the instantaneous velocity fields for lower Re_L looks very similar to their average value, therefore we do not show them.

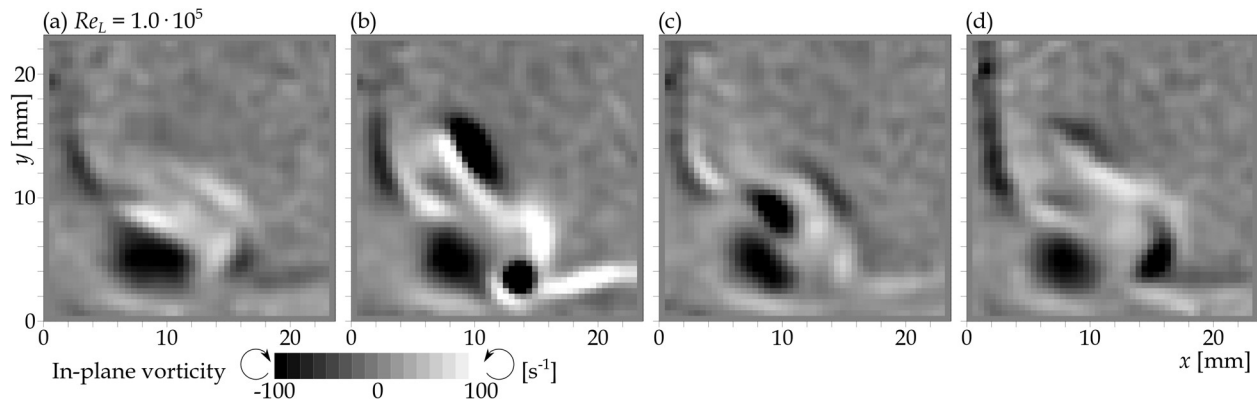


FIGURE 5. Example of instantaneous velocity fields (here is plotted their in-plane vorticity in grayscale) at $Re_L = 1,0 \cdot 10^5$. The *average* of 350 such fields is shown in Figure 3d, the turbulent kinetic energy colored by appropriate length-scale is shown in Figure 6a.

Transition to turbulence

The beginning of transition to turbulence is shown in Figure 5, where we see single laminar vortex in the corner produced by the non-linear interaction of the laminar boundary layers surrounded by other flow structures *induced* by strong shear in the vortex envelope. These structures have not fixed position and also their time of live is questionable (we do not have time-resolved data to judge this issue). They cause, first, the unsteadiness of the parent laminar vortex, which is apparent from plots of diverging standard deviations of its parameters in Figure 4, second at $Re_L = 1,1 \cdot 10^5$ small structures migrate into boundary layer and cause her transition into turbulence. This process is in large detail discussed in another our work.

At even larger Reynolds numbers, the boundary layers are turbulent and the type of interaction changes resulting into loss of single dominant corner vortex. The exact role of the boundary layers needs further investigations, as we are not sure, how this scenario would change, if the boundary layer transitioned into turbulence by another way.

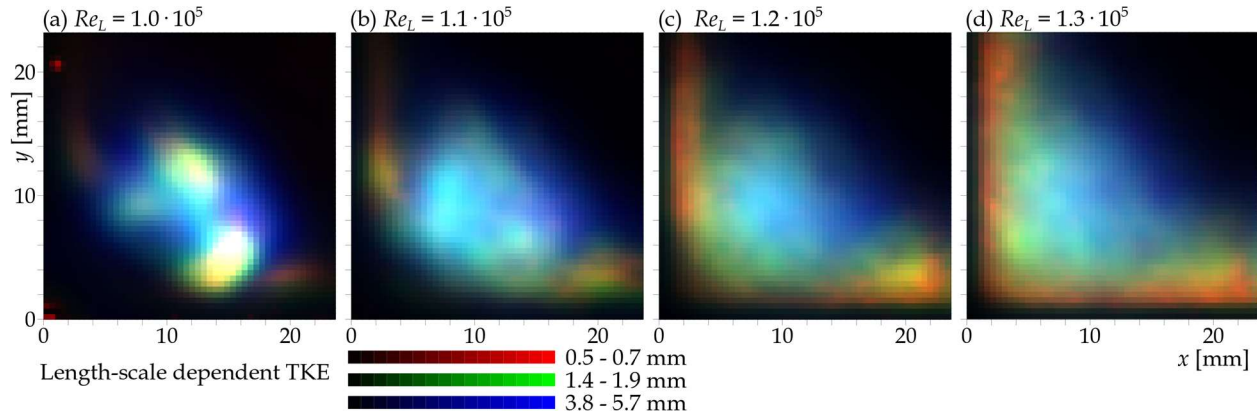


FIGURE 6. Length-scale dependent turbulent kinetic energy at Re_L from $1.0 \cdot 10^5$ to $1.3 \cdot 10^5$, where the transition to turbulence occur. The normalization of energy among different length-scales is by the Kolmogorov $k^{-5/3}$ scaling (i.e. ideal Kolmogorov turbulence would be gray), the normalization among different Reynolds number is by the corresponding fluctuation energy content (i.e. average energy of instantaneous velocity field – energy of average velocity field), which equals $7.0 \cdot 10^{-3} \text{ m}^2\text{s}^{-2}$ for (a), $2.7 \cdot 10^{-2} \text{ m}^2\text{s}^{-2}$ for (b), $8.6 \cdot 10^{-2} \text{ m}^2\text{s}^{-2}$ for (c) and $0.13 \text{ m}^2\text{s}^{-2}$ for (c). Colors correspond to length-scale of the fluctuations, black means no fluctuations, red represents fluctuations at small scale, blue at large scale. We apologize to readers with gray-scale printer.

Turbulent Secondary Flow

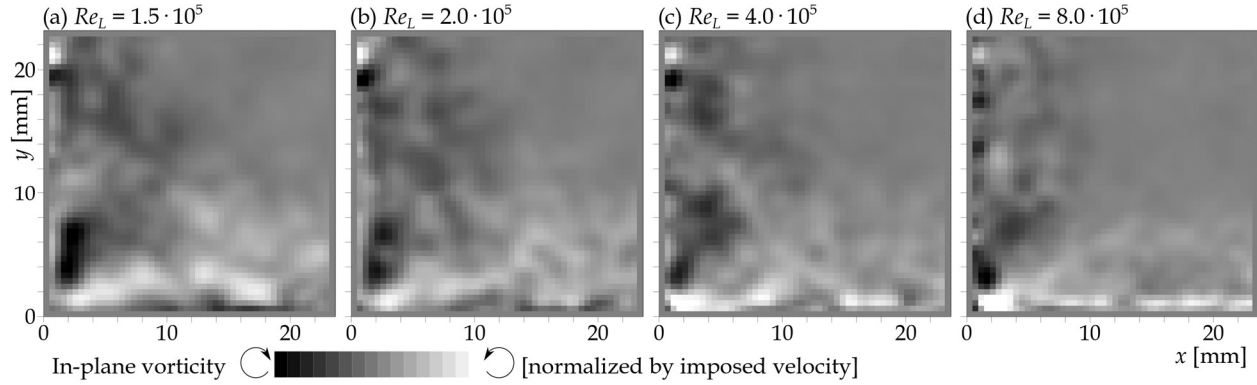


FIGURE 7. Ensemble-averaged spatial distribution of the in-plane vorticity at four different Reynolds numbers in turbulent regime. We apologize for higher noise caused by insufficient averaging (due to the memory limitations we got 350 frame pairs per dataset). We can recognize pair of counter rotating vortices in the corner, whose size slightly decreases with imposed velocity.

In turbulent regime, we observe a pair of counter rotating secondary flow vortices in the corner of the channel as suggested by [5]. In our case this secondary flow in turbulent regime has much smaller size, which has been not observed in the studies of fully developed channel flow, where this structure fills the entire channel cross-section [8].

While in the laminar case, the secondary flow arises due to curving the streamlines by the additional stress in the second boundary layer, in the turbulent case, the secondary flow is related to the *Reynolds stress*, which is naturally connected with the averaging. Therefore, it is not surprise, that there is no trace of this structure in the instantaneous velocity fields, whose example is shown in Figure 8.

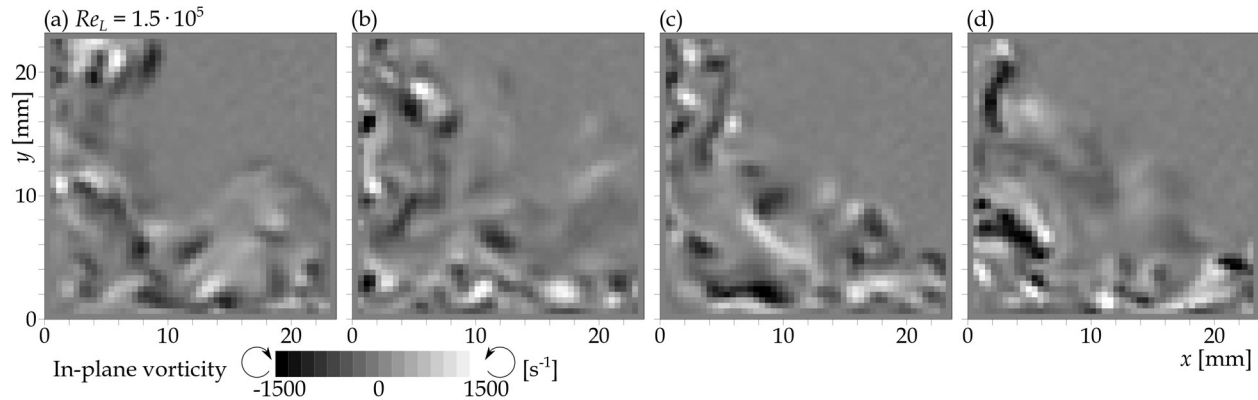


FIGURE 5. Example of instantaneous velocity fields (here is plotted their in-plane vorticity in grayscale) at $Re_L = 1.5 \cdot 10^5$. The average of 350 such fields is shown in Figure 7a. Note, that when comparing with Figure 5 showing instantaneous velocity fields at $Re_L = 1.0 \cdot 10^5$, the vorticity scale is $15\times$ larger, while Re_L is only $1.5\times$ larger.

CONCLUSION

We have observed the *secondary flow of second kind* in the *developing* straight channel flow. If the Reynolds number based on channel length is smaller than $\sim 1.0 \cdot 10^4$, the secondary flow consists of a single laminar vortex rotating clock-wise and thus breaking the symmetry. At $Re_L 1.1 \cdot 10^5$ the fluctuations and vortices produced in the shear region of the corner vortex envelope start to migrate into the boundary layer causing its transition to turbulence spatially starting from the corner. At even larger Re_L the turbulent boundary layers dominate the flow resulting into loss of single corner vortex. There is a pair of smaller counter-rotating vortices in the corner instead, however, they are not apparent in the instantaneous velocity fields, only in the averaged one.

ACKNOWLEDGMENTS

We thank to Ing. Bohumil Laštovka for valuable technical help. This work has been supported by the SGS project No SGS-2019-021.

REFERENCES

1. G. Ilieva “A deep insight to secondary flows”, Defect and Diffusion Forum **379**: 83-107 (2017)
2. W. S. Saric, “Görtler vortices” Annual Review of Fluid Mechanics **26** (1), 379-409 (1994)
3. M. A. Fardin, C. Perge and N. Taberlet, “The hydrogen atom of fluid dynamics – introduction to the Taylor-Coette flow for soft matter scientists”, Soft Matter **10** (20) 3523-3535 (2014)
4. L. S. Langston, “Secondary flows in axial turbines – a review”, Annals of the New York Academy of Sciences **934**: 11-26 (2001)
5. M. Uhlmann, A. Pinelli, G. Kawara and A. Sekimoto, “Marginally turbulent flow in a square duct”, J. Fluid Mech. **588**: 153-162 (2007)
6. M. Hirota, H. Fujita, H. Yokosawa, H. Nakai and H. Itoh, “Turbulent heat transfer in a square duct”, Int. J. Heat and Fluid Flow **18**:170-180 (1997).
7. D. Duda, “Předběžná zpráva o snaze o strojové rozpoznání jednotlivých vírů v PIV datech”, proceedings of the 32th Symposium on Anemometry, 7-13, Litice (2018)
8. V. Uruba, O. Hladík and P. Jonáš, “Dynamics of secondary vortices in turbulent channel flow”, Journal of Physics: Conference Series **318** (6), 062021 (2011)